PHYSICAL REVIEW B VOLUME 45, NUMBER 14 1 APRIL 1992-II

Field and geometry dependence of the ac loss in the critical-state model of type-II superconductors

M. Forsthuber and G. Hilscher
Institut für Experimentalphysik, Technische Universität Wien, Wiedner Hauptstrasse 8-10, A-1040 Wien, Austria
(Received 4 November 1991)

The imaginary part of the ac susceptibility χ'' is studied as a function of varying ac field amplitude and cross-section geometry in the framework of the critical-state model. We present a formalism which allows a straightforward calculation of the position of the maximum of $\chi''(T,H)$. Numerical results demonstrate that, under the assumption of a general power law for the field dependence of j_c, the so-called peak field deviates significantly from the penetration field for the diverse sample cross sections. Consequently the maximum of $\chi''(T,H)$ cannot be considered as an intrinsic property without correcting for the cross section.

I. INTRODUCTION

The investigation of the characteristics of flux motion is one of the main concerns of research on high-T_c superconductors (HTSC's). A major concept in this field is the critical-state model introduced by Bean,[1] by Kim, Hempstead, and Strnad,[2] and by Anderson.[2] According to this model, every part of the sample (except possibly a virgin region at the center of the sample, where no current has been generated) carries a current as high as possible without dissipation. Consequently, the magnetic behavior is governed by the critical-current density j_c; thus the critical-state model has been used to derive the value of the critical-current densities as well as its dependence on the magnetic field. Nevertheless, although it is widely accepted that j_c is strongly influenced by magnetic fields, the analytical form of the dependence is still under discussion.

One of the means to determine the critical-current density of high-T_c superconductors—single crystals as well as ceramics—is the ac susceptibility. Especially the ac loss (which is proportional to the imaginary part χ'' of the ac susceptibility) is of interest and has been used in different ways to determine the value and field dependence of the critical-current density j_c (see, e.g., Refs. 3 and 4); the incentive to this work was Ref. 5, where the attention was focused upon the peak position of χ'' with respect to temperature variation for different fields in order to derive j_c.

In this work we restrict our considerations to homogeneous and isotropic hard type-II superconductors of prismatical or cylindrical shape, whereby the long axis is oriented parallel to the field. We further regard the critical field H_{c1} as negligibly small; the fields regarded here shall be large enough so that $B \approx \mu_0 H$ in the equilibrium, i.e., $\mu_{eq} \approx 1$. We do not take account of surface effects, flux-motion effects [viscous flux flow, thermally activated flux flow (TAFF), etc.], or flux diffusion. Thus we may treat the magnetization cycles occurring during the ac measurement as a sequence of quasistationary processes, as is the case in the critical-state model. Moreover, the exact form of the time dependence of the external field is of no importance for the discussion here; it is sufficient to regard it as a monotonous sweep between the negative and positive field amplitudes.

In this paper we develop a formalism which not only supplies a way to calculate the ac loss for varying field amplitude and sample geometry, but also yields a means to determine the position of the χ'' maximum as a function of these variables with respect to the penetration field. In Sec. II we briefly repeat the general concepts concerning the geometry of flux penetration and critical-state model. Section III introduces the calculus to derive χ'' and to determine the peak state. Then we present the results of our numerical calculations, including the low- and high-field behavior of χ'', for critical-current densities obeying a power-law dependence on the magnetic field (Sec. IV) and conclude with Sec. V. We added an Appendix with analytical results supplementary to Sec. IV.

II. BASIC EQUATIONS

A. Geometry

In general, we consider sample geometries of cylindrical and prismatical shapes, whereby the length of the sample shall be large enough with respect to its lateral dimensions so that we may treat the sample as infinitely long. In particular, rectangular cross sections are studied since they form a representative subset, as we will see below. We identify the long axis with the z axis and assume that the sample is exposed to a homogeneous external field along the z axis. Thus the physical quantities do not depend on the coordinate z, as variations at the end of the sample are small with respect to the bulk and are, therefore, neglected. Hence, we need not consider demagnetization effects.

Thus we are dealing with quantities varying only over the sample cross section. In order to obtain a quasi-one-dimensional description of the critical state, we introduce suitable coordinates for the cross section. For cylindrical samples these are polar coordinates. Rather than the radius, however, we shall take the depth $x = R - r$, which is more appropriate to describe the penetration of flux into

the sample from the surface. The points of constant depth x form concentrical rings of length $c(x)=2\pi(R-x)$. We shall call these rings "perimeters" and apply this term also to their correspondents for other sample geometries. For cross sections which are not circular, we define a perimeter as the line formed by all points at a given depth x from the surface. (See Fig. 1; for a discussion of flux fronts for circular and elliptical cross sections, see also Ref. 6.)

The perimeters of convex polygonal cross sections at a depth x are convex polygons formed by lines parallel to the polygon sides displaced inward by the depth x (omitting all line segments that are cut off at the end). In the case of a rectangular cross section [Fig. 1(b)], the perimeters are rectangles whose side lengths consecutively decrease until we reach the central perimeter, which is reduced to a line, i.e., a rectangle of zero width, at a depth of half the width of the original rectangle ($x=b/2$). The lengths of these rectangular perimeters are given by $c(x)=2a+2b-8x$. For cross-sectional shapes not too unconventional (i.e., for triangles, rectangles including the square, circles, and so forth, but not for, e.g., an ellipse or, even worse, a circle's segment), the lengths of the perimeters, $c(x)$, are given by a linear function of the depth x over the whole range from 0 to the maximal depth R, which corresponds to the central perimeter shrunk to a line or point:

$$c(x)=c_0-c_1x, \quad 0\le x\le R \ , \tag{1}$$

where c_0 is the length of the surface perimeter of the sample and c_1 describes the reduction of the perimeters as one penetrates into the sample. For a circle they are $c_0=2\pi R$ and $c_1=2\pi$, whereas a rectangle with side lengths a and b has $c_0=2a+2b$ and $c_1=8$. We restrict our discussions to cross sections with perimeters (1).

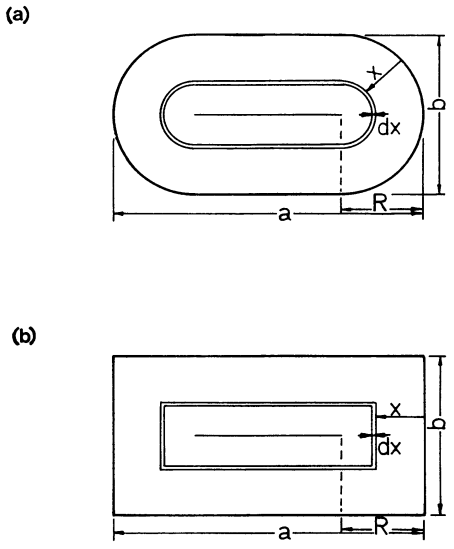

FIG. 1. Cross section of (a) a "round stripe" sample and (b) a rectangular sample with width a and thickness b. Also drawn are two perimeters at depths x and $x+dx$, as well as the central perimeter at the maximal depth R. See the text for further explanations.

The other set of coordinate lines, which are the generalized radii of the circular cross section, is generated by straight lines perpendicular to the perimeters. Note that these quasiradii start at the surface, though not necessarily all of them extend to the central perimeter. In the critical-state model, a quasiradius may be seen as the line along which the flux quanta enter the sample; therefore the flux profile runs along these lines.

Since the physical quantities, such as, e.g., the flux density, are constant over the range of a perimeter within the critical-state model, integration over the cross section is easily performed by adding up the contributions of perimeters using the area element $df=c(x)dx=(c_0-c_1x)dx$, with c_0 and c_1 as defined above.

Thus the geometry of a sample is described by the three parameters c_0, c_1, and R. We define the number

$$\gamma=\frac{c_0}{c_1R} \ , \tag{2}$$

which only depends on the shape but not on the size of the sample. Cross sections with equal γ values are expected to behave equivalently within the framework of the critical-state model. For rectangular samples the shape parameter γ is given by

$$\gamma=\frac{1}{2}\left[\frac{a}{b}+1\right] . \tag{3}$$

B. Critical-state model

In this subsection we repeat the concepts of the critical-state model[1,2] needed for further treatment. We shall write the critical-current density j_c in the form

$$j_c(B)=\frac{a_j}{\mu_0 f(B)} \ . \tag{4}$$

Here we have introduced the function $f(B)$ to describe the field dependence. It is a symmetric [i.e., $f(-B)=f(B)$], non-negative function which, for physical reasons, grows monotonously for $B\ge 0$. a_j is a parameter to describe variations of the critical-current density due to parameters other than the magnetic field. Typically, the variation of a_j is due to changing temperature, i.e., $a_j=a_j(T)$,[4,5] but it may also depend on other parameters, e.g., defect concentration (varied by either alloying or annealing), neutron irradiation,[7] or grain size and morphology of the grains of granular HTSC's.[8] Equation (4) represents the assumption that the dependence with respect to the field can be separated from the remaining other parameters.

With the sample geometries discussed above, the model allows a quasi-one-dimensional description of the current and flux distributions within the sample. Currents will flow along perimeters in the sample since this corresponds to a minimum of penetrated flux within the sample. Flux moves along the quasiradii, mentioned above. Consequently, the flux gradient (flux profile) is appropriately expressed as a function of the surface depth x along the quasiradial lines.

The flux density B obeys Ampère's law with respect to the critical-current density:

$$\pm\frac{dB}{dx}=\mu_0 j_c(B) . \tag{5}$$

In this equation the sign may alternate for subsequent depth intervals. The integration constants are fixed by the surface condition $B(x=0)=\mu_0 H$ for the outermost interval and the continuity $B(x_i-)=B(x_i+)$ for the following intervals, respectively. [If a virgin region exists in the center of the sample, we have $B(x=x_m)=0$ as an additional constraint defining the depth x_m where the virgin region begins.] Using (4), we can integrate (5) and obtain B as a function of x and H:

$$\begin{aligned} &F(B)=F(B_0)\pm a_j(x-x_0) , \\ &B=F^{-1}(F(B_0)\pm a_j(x-x_0)) , \end{aligned} \tag{6}$$

where F is the stem function of f, defined as

$$F(B)\equiv\int_0^B f(B')dB' ,$$

with the inverse function F^{-1}, and the integration constant in (6) is chosen in accordance with the condition $B(x_0)=B_0$ at some depth x_0 in the interval considered.

The sign in (5) and (6) is determined by the sample history: The negative sign is chosen for regions where flux has been moved inward, corresponding to increasing external field; the positive sign marks outward flux motion driven by decreasing external field. Thus, in general, continuous solutions patched together from solutions according to (6) (with alternating signs) are expected when the external field is not a monotonous function of time.

Considering the monotonous flux profile with applied external field H as a special case, we have the negative sign in (6) and $B(x_0=0)=\mu_0 H$; the penetration length $\mathcal{X}(H)$ is defined as the depth at which $B=0$:

$$\mathcal{X}(H)=\frac{1}{a_j}F(\mu_0 H) . \tag{7}$$

Inversely, we define the field yielding a penetration length x as

$$\mathcal{H}(x)=\frac{1}{\mu_0}F^{-1}(a_j x) . \tag{8}$$

When the penetration length of the field amplitude equals the sample depth R, the sample is said to be in the penetrated state and $H_p=\mathcal{H}(R)$ is called the penetration field of the sample.

As mentioned in the Introduction, we are dealing with an ac external field of amplitude H_m. We give the solution for an external field increasing from an initial value $-H_m$; the solution for decreasing field (starting from $+H_m$) is analogous. In general, the solution consists of three parts: (i) an outer region determined by the presently applied external field H, (ii) a region where the flux profile persists as built up by the negative-field amplitude $-H_m$, and (iii) the virgin region:

$$B(a_j x,H)=\begin{cases} \mu_0\mathcal{H}[\mathcal{X}(H)-x], & 0\le x\le x_A(H) \quad \text{(i)} \\ \mu_0\mathcal{H}[-\mathcal{X}(H_m)+x], & x_A(H)\le x\le x_m \quad \text{(ii)} \\ 0, & x_m\le x \quad \text{(iii)} . \end{cases} \tag{9}$$

The "apical" depth x_A and amplitude depth x_m are given by

$$\begin{aligned} &x_A(H)=\tfrac{1}{2}[\mathcal{X}(H)+\mathcal{X}(H_m)] , \\ &x_m=\mathcal{X}(H_m) . \end{aligned} \tag{10}$$

See also Fig. 2 for a schematic flux profile with the respective quantities labeled. [It must be added that (9) describes solutions for any positive value of the depth x and is, of course, applicable only at depths smaller than the sample depth dealt with, i.e., $x\le R$.]

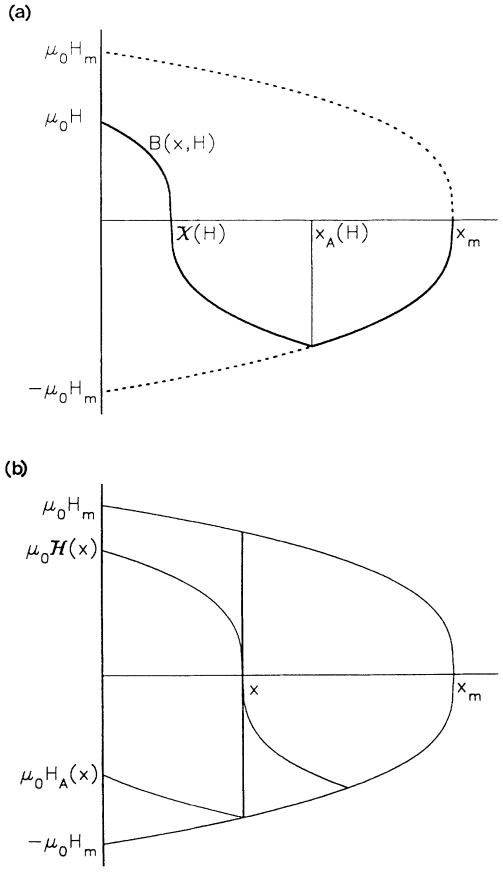

FIG. 2. (a) Flux density B as a function of the depth x for given applied field H (schematic). (b) Graphical definition of the fields $\mathcal{H}(x)$ [see text, Eq. (8)] and $H_A(x)$ [Eq. (23)]. Note that for $H_A(x)$ the field "apex" (the minimum of the flux density) reaches the depth x, while for $\mathcal{H}(x)$ the flux profile crosses the zero level at x.

III. ac LOSS

A. Total and local loss

The magnetic power loss during a cycle caused in a sample by hysteretic behavior is given by[9]

$$W=\int_{(V)}dV\oint_{(H_m)}H\,dB=-\int_{(V)}dV\oint_{(H_m)}B\,dH\ , \qquad (11)$$

where H is the applied external field and B is the flux density in the sample; the volume integration extends over the sample volume, and the circular integral is performed over one magnetization loop with field amplitude H_m. The imaginary part of the complex susceptibility is the normalized power loss[9]

$$\chi''=\frac{W}{\mu_0\pi H_m^2 V}\ , \qquad (12)$$

where H_m is the ac amplitude of the external field and V is the sample volume.

It is useful to perform the integrations of (11) in separate steps. Using the flux density $B(a_j,H)$ of (9), we define the local-loss function

$$w(a_jx,H_m)\equiv-\frac{1}{\mu_0\pi H_m^2}\oint_{(H_m)}B(a_jx,H)dH\ . \qquad (13)$$

Note that the integration variable H is still the *external* field, rather than the local-field strength. In the following we suppress H_m and simply write $w(a_jx)$, although the local-loss function does depend on the value of the field amplitude H_m.

The imaginary part of the ac susceptibility χ'' is the average of the local loss over the sample. For the sample geometries used here having the cross-sectional area $F=c_0R-\frac{1}{2}c_1R^2$,

$$\begin{aligned}\chi''&=\frac{1}{F}\int_0^R dx(c_0-c_1x)w(a_jx)\\&=\frac{2}{2\gamma-1}\left[\frac{\gamma}{R}\int_0^R w(a_jx)dx-\frac{1}{R^2}\int_0^R w(a_jx)x\,dx\right],\end{aligned} \qquad (14)$$

with the geometry parameter γ defined above.

It is obvious that χ'' depends vitally on the magnitude and field dependence of the critical-current density (via w), but also on the value of the sample depth R. It is easy to see, e.g., by substitution $a_jx=\bar{x}$ in the integrals in (14), that χ'' actually depends on the product a_jR rather than on individual a_j and R. Furthermore, (8) directly correlates a_jR to the penetration field H_p. Accordingly, reduction of either the sample thickness or strength of the critical-current density a_j (e.g., by increasing the temperature), as well as an increase of the ac field, essentially has the same effect, which can be described in terms of the increment of the ratio of the field amplitude to the penetration field, H_m/H_p. As discussed in the literature,[9–11] when H_m/H_p grows, χ'' first increases, but reaches a maximum in the range $H_m\sim H_p$, and then decreases to zero again. It is easy to show (see Ref. 9 or the Appendix) that for cylindrical samples in the case of Bean's model ($j_c=a_j=$const) χ'' attains its maximum just at the penetrated state, i.e., when $H_m=H_p$. For other geometries and field dependences, the situation is more complex than this, and the maximum of χ'' may shift to greater or smaller values of H_m/H_p, depending on the values of the quantities mentioned.

B. Peak state

When the imaginary part of the ac susceptibility χ'' attains its maximum for a given sample, the sample is said to be in the peak state. In general, the peak state is different from the penetrated state, and the value of the penetration field H_p can deviate from the peak field H_m^* by a factor of up to $\frac{3}{4}$.[10] We want to derive an expression which correlates the penetration field H_p to the peak field H_m^* for given sample shape as defined by γ and the field dependence of the critical current, $f(B)$.

We are considering changes of the ac loss due to variations of the critical current by, e.g., the temperature, which means that we are varying the critical-current strength a_j [Eq. (4)]. Thus the peak state condition is

$$\frac{d\chi''}{da_j}=0\ . \qquad (15)$$

Hence, using (14),

$$\begin{aligned}0&=a_j\int_0^R dx(c_0-c_1x)\frac{dw(a_jx)}{da_j}\\&=\int_0^R dx(c_0-c_1x)x\frac{d}{dx}w(a_jx)\\&=(c_0R-c_1R^2)w(a_jR)-\int_0^R dx(c_0-2c_1x)w(a_jx)\ ,\end{aligned}$$

since the local-loss function is a function of the product a_jx and the substitution $a_jdw(a_jx)/da_j=xdw(a_jx)/dx$ allows partial integration. We reorder the above equation and obtain an expression using the local-loss function to find the geometry parameter γ for the peak state:

$$\gamma=\frac{c_0}{c_1R}=\frac{w(a_jR)-(2/R^2)\int_0^R w(a_jx)x\,dx}{w(a_jR)-(1/R)\int_0^R w(a_jx)dx}\ . \qquad (16a)$$

For the case that the peak field is smaller than the penetration field, $H_m<H_p$ or, equivalently, $x_m<R$, (16a) can be simplified. Since for depths greater than the penetration length of the peak field, i.e., $x>x_m$, no changes of the flux density occur throughout the whole field loop; the local-loss function vanishes in this region. Thus $w(a_jR)=0$ and both integrations are performed only up to x_m, giving

$$\gamma=\frac{c_0}{c_1R}=\frac{2}{R}\frac{\int_0^{x_m}w(a_jx)x\,dx}{\int_0^{x_m}w(a_jx)dx}\ . \qquad (16b)$$

Equation (16) relates the sample shape characterized by γ to the sample depth R; the parameters, namely, the peak field H_m^* and the field dependence of the critical

current, $f(B)$, are contained in the local-loss function w. Note that the critical-current strength a_j is not a truly independent parameter since both equations effectively contain the product $a_j R$ only. As follows from (8), the sample depth and penetration field are directly related. Thus we can use (16) as an implicit relation to determine the ratio H_m^*/H_p between the peak and penetration fields, for a given sample geometry and field dependence of j_c.

We want to emphasize that (16) determines the parameters γ and R, but poses no additional conditions on the cross-section geometry. For this reason there are cross-sectional shapes equivalent to each other with respect to the peak state. Altogether, rectangles are representative for the entire set of cross sections regarded here, with $R=b/2$ and γ given by (3). For instance, all regular polygons, and the circle (cylindrical sample) as a limiting case, behave in the same way since they all have $\gamma=1$ (or $c_0=c_1 R$), which corresponds to a square cross section.

IV. RESULTS

A. Current dependences investigated

In the literature various forms of field dependences $f(B)$ of the critical-current density have been discussed and used in the context of critical behavior of HTSC's.[12] In this paper we want to discuss critical currents depending on the field according to

$$j_c(B)=\frac{a_j}{\mu_0|B|^\beta} \tag{17}$$

or $f(B)\equiv|B|^\beta$.

This is a special case of the critical-current density

$$j_c(B)=\frac{a_j}{\mu_0|B+b_0|^\beta} \tag{18}$$

[corresponding to $f(B)=|B+b_0|^\beta$], which has been used to describe the field and temperature dependences of the intergranular currents of ceramic HTSC's.[5] Equation (18) represents a generalization of the Kim-Anderson model[2] in that the heuristic field exponent β was introduced. The original Kim-Anderson model corresponds to $\beta=1$ and contains a constant b_0 which serves to avoid the divergency in the low-field behavior of j_c. In Ref. 5, b_0 was found to be rather small in comparison with the fields applied. In this paper we drop this constant, not only for the sake of simplicity, but also for the following reason.

Consider (5) for the field dependence (17),

$$\pm\frac{dB}{dx}=\frac{a_j}{|B|^\beta}\ , \tag{19}$$

which defines the shape of flux profiles according to the critical-state model. If we change the field and spatial scales simultaneously according to

$$\begin{aligned} &B\mapsto B'=\lambda B\ ,\\ &x\mapsto x'=\lambda^{\beta+1}x \end{aligned} \tag{20}$$

(λ is an arbitrary number), (19) still holds with the same value of a_j. For the formalism discussed in this paper, this means that all field scales are equivalent and may be varied freely, as long as the spatial parameters, i.e., R and c_0, are transformed according to (20b). Since the geometry parameter γ (as well as c_1) and field ratio H_m/H_p are dimensionless numbers, they remain unchanged at these transformations. In other words, the ac susceptibility is invariable if the size (but not the shape) of a sample is varied *and* the applied fields are adjusted accordingly. Moreover, the condition for the peak state (16) holds not only for varying critical current [Eq. (15)], but also for varying field amplitude $d\chi''/dH_m=0$: The maximum of χ'' determined by measuring the susceptibility for varying probing field coincides with the one obtained from a temperature-sweep measurement.

If, on the other hand, the critical-current density did obey (18), a field scale would be introduced, viz., b_0, and the scaling symmetry would be broken. The relation between the parameters γ and H_m/H_p would then be governed by the absolute value of the field amplitude H_m in terms of the constant b_0/μ_0, and the maximum of χ'' for varying probing fields cannot be calculated using the above condition (15).

B. Field profiles and local loss

In the following we apply the formalism presented in Sec. III to critical-current densities obeying (17). The penetration length of the applied field (7) and the correlated field (8) attain the form

$$\begin{aligned} &\mathcal{X}(H)=\frac{|H|^\beta H}{\alpha}\ ,\\ &\mathcal{H}(x)=(\alpha|x|)^{1/(\beta+1)}\mathrm{sgn}x\ , \end{aligned}$$

respectively. We use the sign function $\mathrm{sgn}x=|x|/x$ and the abbreviation $\alpha\equiv(\beta+1)a_j/\mu_0^{\beta+1}$. Thus the field profile (9) in the sample reads[13]

$$B(a_j x,H)=\begin{cases}(\mu_0|H|^\beta H-\alpha x)^{1/(\beta+1)}, & x\le\mathcal{X}(H)\\ -\mu_0(\alpha x-|H|^\beta H)^{1/(\beta+1)}, & \mathcal{X}(H)\le x\le x_A(H)\\ -\mu_0^\beta[\alpha(x_m-x)]^{1/(\beta+1)}, & x_A(H)\le x\le x_m\ ,\end{cases} \tag{21}$$

where the intervals are defined by the penetration length of the external field $\mathcal{X}(H)$, the apical depth x_A, and the amplitude depth x_m:

$$x_A(H)=\frac{H_m^{\beta+1}+|H|^{\beta}H}{2\alpha},$$

$$x_m=\mathcal{X}(H_m)=\frac{H_m^{\beta+1}}{\alpha}.$$

[As long as the external field is negative, the first interval vanishes in (21).] With the field profile (21), the local-loss function for a given depth x is

$$\begin{aligned} w(a_j x)&=-\frac{2}{\mu_0\pi H_m^2}\int_{-H_m}^{H_m} B(a_j x,H)\,dH \\ &=-\frac{2}{\pi H_m^2}\left[-[H_A(x)+H_m][\alpha(x_m-x)]^{1/(\beta+1)}+\int_{H_A(x)}^{\mathcal{H}(x)}-(\alpha x-|H|^{\beta}H)^{1/(\beta+1)}dH\right. \\ &\quad\left.+\int_{\mathcal{H}(x)}^{H_m}(H^{\beta+1}-\alpha x)^{1/(\beta+1)}dH\right]. \end{aligned} \tag{22}$$

Each of the integrands of the right-hand side of (22) represents the three intervals of (21) in reversed order. Figure 2(b) displays the flux profiles for the external fields $-H_m$, $H_A(x)$, $\mathcal{H}(x)$, and H_m, which form the boundaries of the integrals in (22). The quantity

$$\begin{aligned} H_A(x)&=\mathcal{H}(2x-x_m) \\ &=(\alpha|2x-x_m|)^{1/(\beta+1)}\mathrm{sgn}(2x-x_m) \end{aligned} \tag{23}$$

corresponds to x_A and denotes the value of the external field at which flux starts to move at the depth x.

The integrals of (22) can be solved analytically for $\beta=0$ or 1 (i.e., Bean's or the Kim-Anderson model) and are given in the Appendix. For other values of the field exponent, only numerical solutions are possible. A computer program written in FORTRAN77 was employed to obtain the local-loss function $w(a_j x)$ in the interval $0<x\le x_m$ for different values of the field exponent, $\beta=0,\ldots,9$. The program also computes the integrals occurring in (14) and (16); and for variable sample depth R, the geometry parameter γ of the peak state is calculated where it is defined (i.e., $\gamma\ge 1$). The results are given in the following sections.

C. ac losses

The imaginary part of the ac susceptibility, χ'', for different values of the field exponent β, was determined from the calculated data mentioned in Sec. IV B using (14). χ'' depends on the value of the field amplitude H_m for given current strength a_j and sample geometries γ and R. For dimensional reasons, however, it is clear that χ'' only depends on dimensionless parameters, namely, γ and H_m/H_p, where $H_p=\mathcal{H}(R)$ (8).

Figure 3 shows the field dependence of χ'' for different field exponents β and different sample geometries; for the sake of lucidity, the sample geometries are expressed in terms of the side ratio b/a of a rectangular cross section. For all values of β, χ'' shows a maximum in the range where $H_m\sim H_p$; for higher as well as for lower field amplitudes, it decreases smoothly (except for a slight kink at $H_m=H_p$) and vanishes asymptotically when H_m decreases to 0 or diverges. As is visible from the inserted log-log plots in Fig. 3, χ'' approaches asymptotical straight lines for $H_m\to 0$ as well as for $H_m\to\infty$. The slopes of these straight lines depend on the respective value of β and are discussed below.

D. ac losses in the low-field limit

In the low-field regime ($H_m\ll H_p$ or $x_m\ll R$), flux penetrates only a small depth from the surface. Therefore we can neglect the second term on the right-hand side of (14), which just takes the reduction of the perimeter lengths at growing depth into account, and keep the first term:

$$\begin{aligned} \chi''\propto R^{-1}\int_0^{x_m} w(a_j x)\,dx&=\frac{x_m}{R}\int_0^1 \bar{w}(\bar{x})\,d\bar{x} \\ &\propto\frac{x_m}{R}\propto\left[\frac{H_m}{H_p}\right]^{\beta+1}, \end{aligned}$$

where we substituted $\bar{x}=x/x_m$ and $\bar{w}(\bar{x})=w(a_j x_m\bar{x})$. The resulting integral does not contain the amplitude depth x_m and is thus a constant (or, strictly speaking, only a function of β). Thus the low-field limit shows the asymptotic power law $\chi''\propto H_m^{\beta+1}$.[13] This can also be seen in the insets of Fig. 3, which are log-log plots: χ'' forms straight lines with a slope $\beta+1$ for $H_m/H_p\ll 1$.

E. ac loss in the high-field limit

To derive the asymptotic behavior of χ'' for high field amplitudes ($H_m\gg H_p$ or $x_m\gg R$), we first consider the local loss (22). We have $x\le R$, and thus $x\ll x_m$. There are two terms that are of interest in this limit. The first term within the large parentheses of (22) yields a contribution proportional to

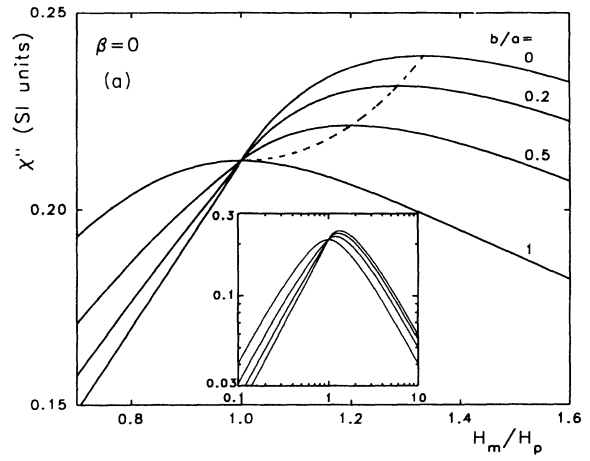

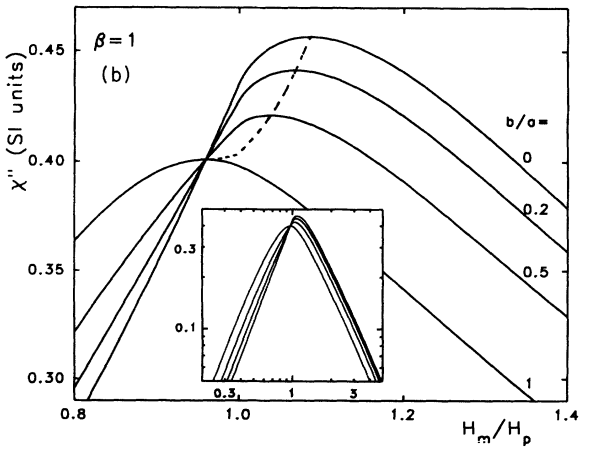

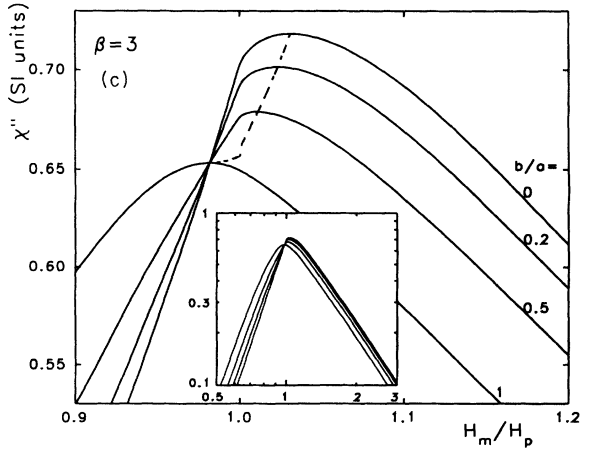

FIG. 3. (a) Imaginary part of the ac susceptibility χ'' (Bean's model, $\beta=0$) as a function of the amplitude of the external field H_m normalized to the penetration field H_p for different side ratios b/a of a rectangular cross section. The dashed line shows the position of the maxima of χ''. Both axes of the inserted graph are logarithmic. (b) The same as (a), but for a critical current obeying $j_c \propto B^{-1}$. (c) The same as (a), but for a critical current obeying $j_c \propto B^{-3}$.

$$w_1 = \frac{2}{\pi}\left[\frac{H_A(x)}{H_m}+1\right]\frac{1}{H_m}[\alpha(x_m-x)]^{1/(\beta+1)}$$

$$\approx \frac{2}{\pi}\frac{2}{\beta+1}\frac{x}{x_m}\left[1-\frac{x}{x_m}\right]^{1/(\beta+1)}$$

$$\propto \frac{x}{x_m},$$

since $\alpha x_m = H_m^{\beta+1}$ and

$$H_A(x) = -H_m\left[1-2\frac{x}{x_m}\right]^{1/(\beta+1)}$$

$$\approx -H_m\left[1-\frac{2}{\beta+1}\frac{x}{x_m}\right].$$

The other main contribution is contained in the second term on the right-hand side of (22):

$$w_3 = \frac{2}{\pi H_m^2}\int_0^{\mathcal{H}(x)}(\alpha x - H^{\beta+1})^{1/(\beta+1)}dH$$

$$= \frac{2}{\pi}\left[\frac{\mathcal{H}(x)}{H_m}\right]^2\int_0^1(1-h^{\beta+1})^{1/(\beta+1)}dh$$

$$\propto \left[\frac{\mathcal{H}(x)}{H_m}\right]^2 \propto \left[\frac{x}{x_m}\right]^{2/(\beta+1)},$$

where we performed the substitution $h = H/\mathcal{H}(x)$ and the integral turns out to be a constant (i.e., a function only of β). To determine the dominating contribution, we have to compare the exponents with respect to the depth x. If $\beta>1$, then $2/(\beta+1)>1$ and w_3 is the dominating term, i.e., $w(a_j x)\propto x^{2/(\beta+1)}$; for $\beta<1$, on the other hand, w_1 dominates the local-loss function, and we then have $w(a_j x)\propto x$.

For the limiting case $\beta=1$, both above formulas predict a high-field dependence $w(a_j x)\propto x$. However, the analytical solution gives

$$w(a_j x)\propto \frac{x}{x_m}\left[1+\frac{\pi}{2}-\ln\left[\frac{x}{x_m}\right]\right]\approx \frac{x}{x_m}\ln\left[\frac{x_m}{x}\right].$$

This result is derived in the Appendix.

It is easy to see from (14) that χ'' retains the high-field exponent of the local loss w; note that R substitutes for x. Thus

$$\chi'' \propto \begin{cases} \dfrac{R}{x_m} = \left[\dfrac{H_p}{H_m}\right]^{\beta+1}, & \beta<1 \\ \dfrac{R}{x_m}\ln\left[\dfrac{x_m}{R}\right] \propto \left[\dfrac{H_p}{H_m}\right]^2 \ln\left[\dfrac{H_m}{H_p}\right], & \beta=1 \\ \left[\dfrac{R}{x_m}\right]^{2/(\beta+1)} = \left[\dfrac{H_p}{H_m}\right]^2, & \beta>1, \end{cases}$$

where we used $\alpha R = H_p^{\beta+1}$ and $\alpha x_m = H_m^{\beta+1}$. Also, see the inserted log-log plots in Fig. 3, where, for $H_m \gg H_p$,

TABLE I. Field ratio $q=H_m^*/H_p$ (the ratio of the field amplitude and penetration field at the maximum of χ'') for different sample cross sections, expressed in terms of the side ratio b/a of a rectangular cross section, and different values of the field exponent β.

β \ b/a	0	0.05	0.1	0.2	0.3333	0.4142	0.5	0.6667	0.8	0.9	1
0.0	1.3333	1.3220	1.3103	1.2857	1.2450	1.2265	1.2000	1.1429	1.0909	1.0476	1.0000
0.2	1.2200	1.2113	1.2031	1.1850	1.1588	1.1415	1.1218	1.0796	1.0411	1.0092	0.9690
0.5	1.1415	1.1354	1.1292	1.1161	1.0972	1.0848	1.0708	1.0411	1.0149	0.9920	0.9569
0.7	1.1130	1.1078	1.1026	1.0915	1.0756	1.0652	1.0536	1.0291	1.0083	0.9876	0.9567
1.0	1.0859	1.0816	1.0774	1.0684	1.0556	1.0473	1.0381	1.0192	1.0040	0.9862	0.9599
1.5	1.0604	1.0572	1.0539	1.0471	1.0375	1.0315	1.0248	1.0114	1.0018	0.9882	0.9670
2.0	1.0462	1.0435	1.0409	1.0354	1.0278	1.0231	1.0179	1.0078	1.0012	0.9910	0.9732
2.5	1.0371	1.0349	1.0327	1.0282	1.0219	1.0180	1.0138	1.0058	1.0010	0.9934	0.9781
3.0	1.0309	1.0290	1.0271	1.0233	1.0179	1.0146	1.0111	1.0045	1.0008	0.9953	0.9819
4.0	1.0231	1.0215	1.0200	1.0171	1.0130	1.0105	1.0079	1.0031	1.0006	0.9978	0.9871
5.0	1.0183	1.0170	1.0159	1.0134	1.0102	1.0082	1.0060	1.0023	1.0005	0.9993	0.9904
7.0	1.0133	1.0120	1.0111	1.0093	1.0070	1.0056	1.0041	1.0015	1.0004	1.0000	0.9941
9.0	1.0099	1.0092	1.0084	1.0071	1.0053	1.0042	1.0031	1.0011	1.0003	1.0001	0.9960

χ'' forms straight lines, with slopes $\beta+1$ or 2 for β smaller or greater than 1, respectively.

F. Peak geometries and peak fields

For the peak state a relation between the sample shape and field ratio $q\equiv H_m^*/H_p$ is supplied by (16). Table I gives the values of the field ratio q for various field exponents β and sample shapes as obtained from our calculations; as above, the latter is given in terms of the rectangular side ratio b/a. The data for the boundary cases $b/a=0$ (slab) and 1 (quadratic cross section) as well as for 0.5 and 0.8 are graphically displayed in Fig. 4. For all values of β, q is a decreasing function of the side ratio b/a. Only for Bean's model does $q\geq 1$ hold for all geometries, and it takes values between 1 and $\frac{4}{3}$. For $\beta>0$ the behavior of q is as follows. At $b=0$ the value of q decreases continuously from $\frac{4}{3}$ with growing β, whereas at $b/a=1$ it first decreases, attains a minimum of 0.9564 for $\beta=0.60$, and increases again toward 1. For high values of β, the field ratio q converges to 1 for all geometries. In Fig. 5 the dependence of the peak field H_m^* is shown as a function of the sample side ratio a/b. H_m^* is normalized to the penetration depth H_p, yielding the field ratio q.

In the above discussion of H_m^*, it is implicitly assumed that the width a of the sample (which we assume to be rectangular) is changed, but the thickness b is kept constant to ensure that H_p remains unchanged. However, if the sample thickness $b=2R$ is varied with constant sample width, the penetration depth varies as well. Thus the absolute value of the peak field as a function of the sample thickness is

$$H_m^*(b)=qH_p(b)=q(b/a)\mathcal{H}(b/2)\ . \tag{24}$$

This is shown in Fig. 6; the peak field is given in terms of the penetration field of the corresponding quadratic sample ($b=a$), H_m^0. Note that, while the field ratio q monotonously decreases for growing side ratio b/a (Fig. 5), the peak field H_m^* now increases since the growing penetration field overcompensates the reduction of q. The value

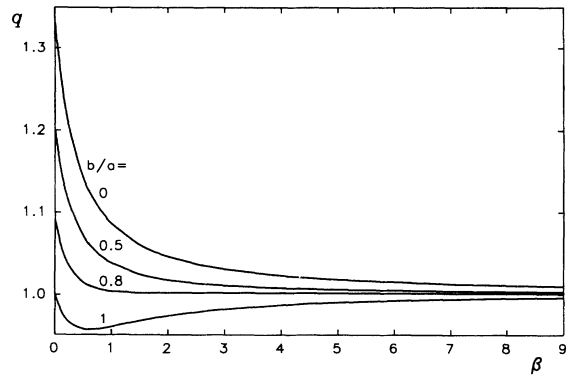

FIG. 4. Field ratio $q=H_m^*/H_p$ (the ratio of the field amplitude and penetration field at the maximum of χ'') as a function of the field exponent β for different side ratios b/a of a rectangular cross section.

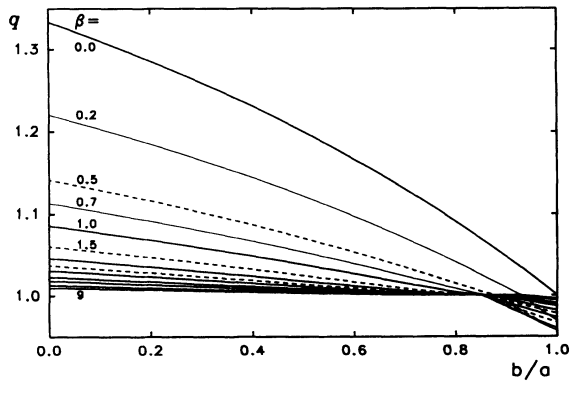

FIG. 5. Field ratio $q=H_m^*/H_p$ (the ratio of the field amplitude and penetration field at the maximum of χ'') as a function of the side ratio b/a of a rectangular cross section for different values of the field exponent β. The values of β where not given in the figure are 2, 2.5 (dashed line), 3, 4, 5, and 7.

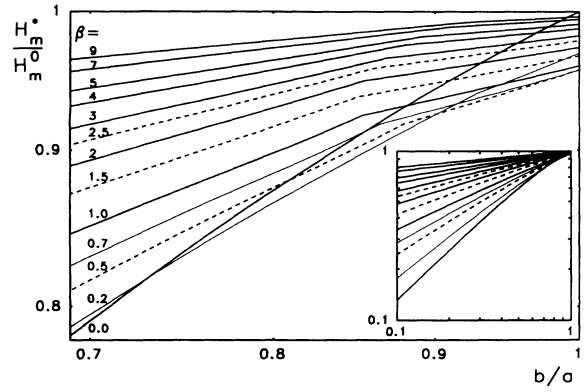

FIG. 6. Peak field H_m^* as a function of the side ratio b/a of a rectangular cross section with constant width a for different values of the field exponent β. The peak field is normalized to H_m^0, the penetration field for $b/a=1$.

of H_m^* starts from 0 for $b=0$ (i.e., a vanishingly thin sample) and increases up to the value $q H_m^0$ for $b=a$ (a quadratic sample). It should be noted that in (24) we used the scaling property (20) for the penetration field H_p and sample depth R.

These results, especially the data of Fig. 6, have been used to determine the field dependence of the critical current in Ref. 5, where we measured the ac susceptibility as a function of the temperature not only for different values of the applied ac field, but also for varying sample thickness. Field exponents β were determined by finding a fit of the experimental data to the calculations presented here. More specifically, the experimental data for constant temperature but different sample cross sections should, when scaled in an appropriate manner, arrange along a line in Fig. 6; this indicates the field exponent β of the critical-current density.

V. CONCLUSION

The imaginary part of the ac susceptibility χ'' depends not only on the amplitude of the external field, but also on the sample geometry. This result is discussed here for sample shapes of vanishing demagnetization factor, i.e., long samples parallel to the field. For more complex geometries (i.e., for nonvanishing demagnetization factor), calculations are not trivial since a quasi-one-dimensional description is not possible. In those cases it is obvious that the geometry dependence will be more pronounced than discussed here.

The geometry dependence of χ'' is most pronounced in the case of a field-independent critical-current density (Bean's model). If a field dependence of the critical-current density is "switched on," i.e., if the field exponent β increases, the geometry dependence of the ratio of the peak and penetration fields, H_m^*/H_p, gradually decreases. For all geometries H_m^* first decreases on rising β from 0, so that for the geometries with small γ (i.e., $\gamma \gtrsim 1$ or $a \gtrsim b$) H_m^* reaches a minimum value below H_p; the minimal value $H_m^*/H_p=0.9564$ occurs at $\beta=0.60$ and $\gamma=1$. For values of β distinctly greater than 1, H_m^* approaches the value of H_p for all geometries. For large β values, the discrepancy between H_m^* and H_p is only a few percent.

In the low- and high-field limits ($H_m \ll H_p$ and $H_m \gg H_p$, respectively), the behavior of χ'' as a function of the field amplitude is independent of the sample geometry and exhibits a power law with respect to H_m. The exponent is $\beta+1$ in the low-field limit,[3] whereas in the high-field limit it is $-(\beta+1)$ for $\beta<1$ and -2 for $\beta>1$.

Our results are calculated under the assumption that $\mu_{\rm eq}=1$. The extension to values for $\mu_{\rm eq}$ other than 1 is straightforward as long as it can be regarded as constant in the field range covered by the values of H_m: the flux density B, and consequently the local-loss function w, and the imaginary part of the ac susceptibility χ'' are reduced by a factor equal to $\mu_{\rm eq}$. This method can also be applied to the intergranular transition of granular HTSC's using the effective permeability $\mu_{\rm eff}$.[4]

Finally, one has to be rather careful if the field and temperature dependences of χ'' are compared for different sample cross sections. In particular, it is noteworthy that the peak of $\chi''(H,T)$ (which several authors used to determine the irreversibility line) cannot be regarded as an intrinsic property of the material without correcting for the influence of the sample cross section. We recommend that in measurements of the ac susceptibility, as far as the maximum of the imaginary part is used in the analysis of data, only quadratic or cylindrical samples should be used since then the possible error due to the field ratio $q=H_m^*/H_p$ is smaller than 5%.

ACKNOWLEDGMENTS

The authors want to thank F. Ludwig, HU Berlin, for highly valuable discussions. This work was supported by the Austrian Science Foundation Funds (Fonds zur Förderung der Wissenschaftlichen Forschung) under Project No. 8173.

APPENDIX

1. Bean's model

The field-independent critical-current density of Bean's model[1] is the limiting case of (17) for $\beta=0$. We repeat the calculations of Sec. IV here in short for $\beta=0$ giving the analytical results.

The local-loss function (22) is

$$w(a_j x)=-\frac{2}{\pi H_m^2}\left[-2\alpha x(H_m-\alpha x)+\int_{2\alpha x-H_m}^{H_m}(H-\alpha x)\,dH\right]$$
$$=\frac{4}{\pi}\frac{\alpha x}{H_m}\left[1-\frac{\alpha x}{H_m}\right].$$

Note that $\mathcal{H}(x)=\alpha x$ and $H_A(x)=\alpha(2x-x_m)$, with

$\alpha=a_j/\mu_0$. The determination of χ'' according to (14) is straightforward and yields

$$\chi''=\frac{2/3\pi}{2\gamma-1}\times\begin{cases}\dfrac{H_m}{H_p}\left[2\gamma-\dfrac{H_m}{H_p}\right], & H_m\le H_p \quad \text{(A1a)}\\ \dfrac{H_m}{H_p}\left[2\gamma\left[3-2\dfrac{H_m}{H_p}\right]+3\dfrac{H_m}{H_p}-4\right], & H_m\le H_p\ . \quad \text{(A1b)}\end{cases}$$

This is given graphically in Fig. 3(a).

For the determination of the peak state, we can use (A1) directly instead of (16). First we note that the slope of χ'' is positive for all $H_m<H_p$; thus we consider only the derivative of (A1b),

$$\frac{d\chi''}{da_j}\propto\frac{d\chi''}{dx_m}\propto\gamma^*\left[3-4\frac{H_p}{H_m}\right]+3\frac{H_p}{H_m}-2=0\ ,$$

from which

$$q=\frac{4\gamma-3}{3\gamma-2}=2\frac{2-b/a}{3-b/a}\ . \quad \text{(A2)}$$

We enter this into (A1) and obtain the maximum value of χ'' as a function of the sample geometry:

$$\chi''_*=\frac{2}{3\pi}\frac{(3\gamma-2)^2}{(2\gamma-1)(4\gamma-3)}=\frac{2}{3\pi q(2-q)}\ . \quad \text{(A3)}$$

The dashed lines in Fig. 3(a) connect the positions of the χ'' maxima for varying q.

Equations (A2) and (A3) yield the well-known results $q=1$ and $\chi''_*=2/3\pi=0.2122$ for cylindrical geometry ($a=b$),[9] whereas $q=4.3$ and $\chi''_*=3/4\pi=0.2387$ for slab geometry ($b\to 0$). Between these limiting cases the field ratio increases monotonously with growing γ (falling b/a); likewise, the maximal value χ''_* increases.

2. Kim-Anderson model with $b_0=0$

In this section we only derive the analytical form of the local-loss function (22) with $\beta=1$ in order to discuss the high-field behavior of χ''. The further calculations are in principle to perform analytically, but are tedious. The local-loss function for $\beta=1$ is as follows. For $x<x_m/2$ we have

$$w(a_j x)=-\frac{2}{\pi H_m^2}\left[-[H_A(x)+H_m]\sqrt{\alpha(x_m-x)}+\int_{H_A(x)}^{0}-(\alpha x+H^2)^{1/2}dH\right.$$
$$\left.+\int_0^{\mathcal{H}(x)}-(\alpha x-H^2)^{1/2}dH+\int_{\mathcal{H}(x)}^{H_m}(H^2-\alpha x)^{1/2}dH\right]$$
$$=\frac{1}{\pi}\left[1-\frac{x}{x_m}\right]^{1/2}\left[1-\left[1-2\frac{x}{x_m}\right]^{1/2}\right]+\frac{x}{\pi x_m}\left[\frac{\pi}{2}+\operatorname{arcsinh}\left[\frac{x_m}{x}-2\right]^{1/2}+\operatorname{arccosh}\left[\frac{x_m}{x}\right]^{1/2}\right], \quad \text{(A4a)}$$

with the notation

$$\alpha=2a_j/\mu_0^2,\quad x_m=H_m^2/\alpha,\quad \mathcal{H}(x)=\sqrt{\alpha x}\ ,\quad H_A(x)=\sqrt{\alpha|x_m-2x|}\ .$$

For $x>x_m/2$,

$$w(a_j x)=-\frac{2}{\pi H_m^2}\left[-\left[H_A(x)+H_m\right]\sqrt{\alpha(x_m-x)}+\int_{H_A(x)}^{\mathcal{H}(x)}-(\alpha x-H^2)^{1/2}dH+\int_{\mathcal{H}(x)}^{H_m}(H^2-\alpha x)^{1/2}dH\right]$$
$$=\frac{1}{\pi}\left[1-\frac{x}{x_m}\right]^{1/2}\left[1+\left[2\frac{x}{x_m}-1\right]^{1/2}\right]+\frac{x}{\pi x_m}\left[\arccos\left[2-\frac{x_m}{x}\right]^{1/2}+\operatorname{arccosh}\left[\frac{x_m}{x}\right]^{1/2}\right], \quad \text{(A4b)}$$

with the same notation as above.

We now are able to discuss the behavior of the local loss in the high-field limit, which means that we consider depths $x\ll x_m$. We can then use the approximation that, for $z\ll 1$,

$$\operatorname{arcsinh} z^{-1/2}\approx\operatorname{arccosh} z^{-1/2}\approx\approx-\tfrac{1}{2}\ln z\ ,$$

and (A4a) simplifies to

$$w(a_j x)\approx\frac{x}{\pi x_m}+\frac{x}{\pi x_m}\left[\frac{\pi}{2}+\ln\left[\frac{x_m}{x}\right]\right]\propto\frac{x}{x_m}\left[C-\ln\left[\frac{x}{x_m}\right]\right]\ . \quad \text{(A5)}$$

For further discussion see Sec. IV.

[1]C. P. Bean, Rev. Mod. Phys. **36**, 31 (1964); Phys. Rev. Lett. **8**, 250 (1962).
[2]Y. B. Kim, C. F. Hempstead, and A. R. Strnad, Phys. Rev. Lett. **9**, 306 (1962); P. W. Anderson, Phys. Rev. Lett. **9**, 309 (1962).
[3]F. Irie and K. Yamafuji, J. Phys. Soc. Jpn. **23**, 255 (1976).
[4]K.-H. Müller, Physica C **159**, 717 (1989).
[5]M. Forsthuber, F. Ludwig, and G. Hilscher, Physica C **177**,

401 (1991).
[6]A. M. Campbell and J. E. Evetts, Adv. Phys. **21**, 199 (1972).
[7]H. W. Weber and G. W. Crabtree, in *Studies of HTSC,* edited by A. V. Narlikar (Nova Science, New York, 1991), Vol. 9.
[8]M. Reissner, W. Steiner, R. Stroh, S. Hörhager, W. Schmid, and W. Wruss, Physica C **167**, 495 (1990).
[9]J. R. Clem (unpublished).
[10]M. N. Wilson, *Superconducting Magnets* (Oxford University Press, New York, 1983).
[11]F. Gömöry and P. Lobotka, Solid State Commun. **66**, 645 (1988).
[12]See, e.g., H. Dersch and G. Blatter, Phys. Rev. B **38**, 11 391 (1988); P. Chaddah, G. Ravi Kumar, A. K. Grover, C. Rhadakrishnamurty, and G. V. Subba Rao, Cryogenics **29**, 907 (1989); V. Calzona, M. R. Cimberle, C. Ferdeghini, M. Putti, and A. S. Siri, Physica C **157**, 425 (1989); and Ref. 4.
[13]I. M. Green and P. Hlawiczka, Proc. IEEE **114**, 1329 (1967).